IOP Publishing Physica Scripta
Phys. Scr. 95 (2020) 035801 (8pp) https://doi.org/10.1088/1402-4896/ab56cd

Zr vacancies and their complexes with hydrogen in monoclinic zirconia: formation energies and positron lifetimes

A G Marinopoulos[1] **and P M Gordo**

CFisUC, Department of Physics, University of Coimbra, P-3004-516 Coimbra, Portugal

E-mail: marinop@uc.pt

Received 14 August 2019, revised 31 October 2019
Accepted for publication 12 November 2019
Published 28 January 2020

Abstract

Cation vacancies in metal oxides have high formation energies and, thus, are not as abundant as their oxygen-related counterparts. Nonetheless, they can be readily created during non-equilibrium processes. Positron-annihilation spectroscopy (PAS) is a well suited technique of probing such defects since negatively-charged lattice vacancies are deep potential wells which can act as positron traps. The present study reports first-principles calculations of positron trapping at Zr monovacancies in monoclinic zirconia. The binding of positrons and associated lifetimes for these defects were obtained within two-component density-functional theory under different approximations for the electron–positron correlation. The role of hydrogen was also explored. Low-energy vacancy–hydrogen defect complexes were determined for one and two hydrogen atoms bound to a single Zr monovacancy. Hydrogen decoration of the vacancy affected the localization of the positron leading to an appreciable decrease of the lifetime. The study was supplemented with PAS measurements on samples of monoclinic zirconia. From the PAS data two distinct, high-intensity components were resolved originating from different defect states. The corresponding lifetimes of 187 and 225 ps were very close to the theoretical predictions.

Keywords: positron annihilation, zirconium oxide, *ab initio* calculations, vacancies, hydrogen

(Some figures may appear in colour only in the online journal)

1. Introduction

Zirconia (ZrO_2) is a wide-gap insulator with diverse uses in many technological processes as a structural ceramic [1]. In recent years monoclinic ZrO_2 has been widely considered in microelectronics as one of the candidate high-κ oxides to replace SiO_2 as the main gate dielectric [2]. Reliability issues related to charge trapping [3] have motivated many computational studies of the intrinsic defects of this material by means of density-functional theory [2, 4–6]. The focus of these studies has been the defects of the oxygen sublattice with the oxygen vacancy widely considered as the dominant electron trap [2]. Cation related defects were found to cost more energy [2, 4, 6], therefore, they must be present in very low concentrations at conditions of thermodynamic equilibrium. Nonetheless, the existence of sizeable concentrations of Zr vacancies has been verified in various zirconia phases, where these defects were created during irradiation or other non-equilibrium treatments [7–9]. One of the most efficient spectroscopies for studying vacancy-type defects in solids is positron-annihilation spectroscopy (PAS) [10–12]. Owing to the missing nuclei at their core such defects can become strong trapping sites for positrons while these thermalize inside the materials [12]. Furthermore, the smaller electron density at open-volume defects leads to a reduced overlap with the positronic density and increases the positron lifetimes measured experimentally by PAS [12].

The present study employed both theoretical and experimental approaches to investigate positron trapping at Zr monovacancies in monoclinic zirconia. The theoretical part consisted of first-principles calculations based on two-component density-functional theory [13–15]. Corresponding positron lifetimes for Zr-vacancy defects were obtained using

[1] Author to whom any correspondence should be addressed.

different approximations for the electron–positron correlation. Experimentally, positron trapping at defects was studied by means of PAS measurements on bulk nanocrystalline powder samples. One of the goals has been to study the effect of hydrogen. Earlier PAS studies in both metals and oxides showed that hydrogen decoration of vacancies can lead to shortening of the positron lifetimes [16–19]. Hydrogen is a ubiquitous impurity in oxides and can have a strong impact on their properties. Its electrical activity, in particular, as an isolated interstitial defect has been the subject of theoretical studies [20–23]. Hydrogen also possesses a strong tendency to associate with oxygen vacancies by occupying their sites and form multi-center bonds with the neighboring metal atoms [24]. The binding of hydrogen to cation vacancies in other zirconia phases [19, 25, 26] and in a number of transparent conducting oxides has also been confirmed by *ab initio* calculations [27]. In monoclinic zirconia nothing is known about how hydrogen interacts with Zr vacancies. The present work addresses this issue, first by determining the energetics of complexing of Zr monovacancies with one and two hydrogen atoms, and secondly by examining how hydrogen affects the interaction of these vacancies with positrons.

2. Theoretical background and experimental preliminaries

Zirconia crystallizes in a monoclinic phase (space group $P2_1/c$) at ambient conditions, with the following lattice parameters determined from experiment [28]: $a = 5.15$ Å, $b = 5.20$ Å, $c = 5.32$ Å and $\beta = 99.20°$. A $2 \times 2 \times 2$ repetition of the primitive 12-atom cell along the three lattice vectors leads to a larger 96-atom supercell which was subsequently used for all defect calculations in the present study. The ground-state structures and corresponding formation energies of Zr vacancies and their complexes with hydrogen were determined by means of density-functional theory [29, 30] and the projected augmented-wave (PAW) method [31]. Both the local-density approximation (LDA) and the generalized-gradient approximation (GGA) were employed to describe electron exchange and correlation effects [32, 33]. The LDA PW92 [32] and the GGA PBE [33] functionals were chosen for this purpose. These calculations were carried out using the VASP *ab initio* code [34–37]. The crystalline wavefunctions were represented by an expansion over plane waves which was limited by a kinetic-energy cutoff of 470 eV. For Zr atoms the semi-core 4*s* and 4*p* states were treated as valence states. The structural optimization for the bulk 12-atom cell was performed using a $4 \times 4 \times 4$ Monkhorst–Pack **k**-point mesh [38] for all integrations over the Brillouin zone. The lattice parameters determined by means of the LDA PW92 functional were equal to: $a = 5.09$ Å, $b = 5.18$ Å, $c = 5.25$ Å and $\beta = 99.52°$. A broader, $2 \times 2 \times 2$ **k**-point mesh was employed in all defect calculations with the larger 96-atom supercell.

The formation energies, $\Delta E^{\rm def}_{\rm form}$, of the Zr monovacancy, $V_{\rm Zr}$, and of the vacancy–hydrogen defect complex, ($V_{\rm Zr}$–H), were determined as a function of the Fermi level, $E_{\rm F}$, and the elemental chemical potentials, $\mu_{\rm Zr}$ and $\mu_{\rm H}$, according to:

$$\Delta E^{\rm def}_{\rm form}(q) = E^{\rm def}_{\rm tot}(q) - E^{\rm bulk}_{\rm tot} + \mu_{\rm Zr} - n\mu_{\rm H} + qE_{\rm F}. \quad (1)$$

In this expression, $E^{\rm def}_{\rm tot}$ and $E^{\rm bulk}_{\rm tot}$, are the total energies of the defect and perfect-lattice supercells, respectively. q is the charge of the defect. n is an integer which takes the value of 0 or 1 for the Zr monovacancy and vacancy–hydrogen complex, respectively. $E_{\rm F}$ is the Fermi level, referenced by the valence-band maximum, E_V, of the bulk supercell. The values of $E_{\rm F}$ span the whole band gap. The latter was found equal to 3.63 eV when employing the LDA PW92 functional. The chemical potentials $\mu_{\rm Zr}$ and $\mu_{\rm H}$ of the two species are referenced with respect to their values in their stable standard states: the bulk hcp Zr metal and the H_2 gas, respectively.

As usually done for intrinsic defects in oxides [27, 39] the formation energies of the vacancy defects were determined for the two extreme limits of the chemical potentials of the cation and oxygen species. These limits are dictated by the values of these potentials in their respective stable states: $\mu^{\rm o}_{\rm Zr}$ (in metallic Zr) and $\mu^{\rm o}_{\rm O}$ (in O_2 gas). These values are upper bounds for $\mu_{\rm Zr}$ and $\mu_{\rm O}$. For Zr-rich conditions: $\mu_{\rm Zr} = \mu^{\rm o}_{\rm Zr}$, and for O-rich conditions: $\mu_{\rm O} = \mu^{\rm o}_{\rm O}$. $\mu_{\rm Zr}$ and $\mu_{\rm O}$ also obey the equilibrium equation: $\mu_{\rm Zr} + 2\mu_{\rm O} = \Delta H_{\rm form}[{\rm ZrO_2}]$, where $\Delta H_{\rm form}[{\rm ZrO_2}]$ is the formation enthalpy of the monoclinic zirconia phase. The magnitude of $\Delta H_{\rm form}[{\rm ZrO_2}]$ was found equal to -13.96 eV per formula unit, using the present LDA functional. In the vacancy–hydrogen defect complex the value of $\mu_{\rm H}$ is further related to the formation enthalpy of water, $\Delta H_{\rm form}[{\rm H_2O}]$, according to: $2\mu_{\rm H} + \mu_{\rm O} < \Delta H_{\rm form}[{\rm H_2O}]$.

The positron lifetimes and corresponding binding energies to the vacancy defects in the present study were determined by means of two-component density-functional theory (TCDFT) [13–15] as implemented in the ABINIT code [40]. Within TCDFT the total energy of the composite system of electrons (of density $n_-(\mathbf{r})$) and the positron (of density $n_+(\mathbf{r})$) under the influence of an external potential $V_{\rm ext}$ is given by [15]:

$$E[n_-, n_+] = F[n_-] + F[n_+] + \int d\mathbf{r}\ V_{\rm ext}(\mathbf{r})[n_-(\mathbf{r}) - n_+(\mathbf{r})] - \iint d\mathbf{r}d\mathbf{r}' \frac{n_-(\mathbf{r})n_+(\mathbf{r})}{|\mathbf{r} - \mathbf{r}'|} + E_c^{e-p}[n_-, n_+], \quad (2)$$

where $F[n]$ stands for the DFT single-component functional of either density and $E_c^{e-p}[n_-,n_+]$ for the electron–positron correlation energy. $E_c^{e-p}[n_-,n_+]$ was determined within the parametrization of Puska, Seitsonen and Nieminen (PSN) which uses a full LDA electron–positron functional [41]. The adopted implementation is based on the PAW formalism for the electron and positron states where both the $n_-(\mathbf{r})$ and $n_+(\mathbf{r})$ densities, respectively, are simultaneously converged to self-consistency [42]. For selected cases, the positron-induced forces on the ions were also taken into account as *a posteriori* corrections. Using these forces an additional energy minimization was conducted and both electron and positron densities were converged for each ionic step. The PAW data sets for the wavefunctions in the solid were generated by the

Table 1. Positron lifetimes, τ_i, and intensities, $I_i(\%)$, measured in monoclinic compacted nanopowder samples. Standard deviations are given in parentheses in units of the last significant digit. It was assumed in all decompositions, the contribution of p-Ps with a fixed lifetime of 0.125 ns and relative intensity of $(I_3 + I_4)/3$.

Samples	τ_1 (ns)	I_1 (%)	τ_2 (ns)	I_2 (%)	τ_3 (ns)	I_3 (%)	τ_4 (ns)	I_4 (%)
HDZ powder	0.187(1)	74.6(5)	0.433(6)	23.8(5)	1.9(1)	0.3(2)	20(1)	0.9(1)
EDS powder	0.225(1)	70.6(9)	0.468(5)	25.0(1)	2.0(1)	0.5(2)	28(1)	2.9(1)

ATOMPAW code [43]. The positronic and electronic wavefunctions were expressed using the same basis [40, 42].

The final converged positron and electron densities, $n_+(\mathbf{r})$ and $n_-(\mathbf{r})$, respectively, were used to calculate the probability of annihilation and the positron lifetime, τ. The latter is obtained as follows [15]:

$$\frac{1}{\tau} = \pi c r_o^2 \int d\mathbf{r}\, n_+(\mathbf{r})\, n_-(\mathbf{r})\, g(n_+, n_-), \tag{3}$$

where c is the speed of light and r_o the classical radius of an electron. The $g(n_+,n_-)$ term is the enhancement factor which accounts for the screening in the solid and the increase in the electron density at the positron site [15]. In the present study the parametrization proposed by PSN was chosen [41], whereby functional forms for $g(n_+,n_-)$ were constructed which interpolate within a two-dimensional plane of electron and positron densities [15].

Additional calculations were further performed adopting a gradient-correction (GC) scheme [44, 45] which incorporates the effects of the nonuniform electron density in both the enhancement factor and the electron–positron correlation energy [40]. In this case the atomic positions were optimized by means of the GGA-PBE functional.

Two different commercial samples of pure monoclinic zirconia in nanosized-powder form were investigated in the present work. One of the samples was manufactured by Alfa Aesar Company and the other by Innovnano Company. Both of them had a pure ZrO_2 monoclinic phase, as verified by x-ray diffraction. The two samples were manufactured by different synthesis methods. In the case of the sample from Alfa Aesar the powder was obtained from the hydrolysis of Zr (to be referred to as HDZ from now on), while the powder from Innovnano was produced via emission detonation synthesis (EDS technology). To prepare the samples the powders were pressed at room temperature into tablets of 15 mm diameter and 5 mm thickness. A pressure of about 100 MPa was applied. The mean grain size of our samples was determined from the broadening of the x-ray diffraction lines by using the Scherrer formula. Values of 17(1) nm and 57(5) nm were obtained for the EDS and HDZ samples, respectively.

The PAS-data acquisition was achieved via a positron source of about 0.4 MBq that was made of ^{22}NaCl water solution (Perkin Elmer) dried and sealed between 10 μm Kapton γ foils (DuPont). A fast-fast coincidence circuit of the PAS setup (featuring BaF_2 scintillators and Hamamatsu R3378 photomultipliers), with a time resolution of approximately 200 ps (full width at half maximum, FWHM, for ^{22}Na), was used to record the positron lifetime spectra. The positron ^{22}Na source was sandwiched between two identical samples. Several spectra were collected at room temperature. The lifetime spectra had at least 4×10^6 of integral counts. Each spectrum was decomposed into individual discrete components by means of the LT software (version 9) [46]. The fraction of positrons that annihilates in the source and covering foils, the so-called source contribution, was determined for a well annealed pure crystalline silicon sample (with bulk lifetime of 218 $\pm$ 1 ps). The source contribution was recalculated for the zirconia samples used in this work according to the method described in [47].

3. Results and discussion

3.1. Perfect-lattice calculations

The positron lifetime, τ_{bulk}, for the perfect-lattice (bulk) monoclinic supercell was determined in the zero-density positron limit, using both the PSN and the GC schemes, and with the lattice parameters fixed to their experimental values. The latter condition was enforced in order to ensure appropriate comparisons with the PAS data, since lifetimes depend upon the average electron density [48]. Furthermore, owing to the complete delocalisation of the positronic density in the entire supercell only the Γ **k** point was employed [40]. The corresponding lifetimes were found equal to 152 and 179 ps by the PSN and GC methods, respectively. These values compare well to the results of an earlier TCDFT study [7] for the monoclinic phase of zirconia where the atomic-superposition (ATSUP) method was adopted; the reported lifetimes for the perfect lattice were 160 and 170 ps using an LDA and a GC-based electron–positron correlation scheme [15], respectively. The ATSUP methodology does not account for charge-transfer effects when constructing the effective electron and positron potentials, and this probably explains the differences with the present lifetime values.

3.2. Experimental PAS measurements

The lifetime spectra of the zirconia powders were decomposed into four exponential components, each characterized by a positron lifetime, τ_i, with a certain intensity, I_i, $(\sum I_i = 1)$. The positron source contribution and para-positronium (p-Ps) component were subtracted from the spectra. The resulting lifetimes, τ_i, and intensities, I_i, are summarized in table 1 for both HDZ and EDS samples.

The results in table 1 show that both samples comprise two groups of positron lifetimes: the long lifetime group (lifetimes above 1 ns) with the τ_3 and τ_4 components, and the short lifetime group (lifetimes below 1 ns) with the τ_1 and τ_2 components. The intensities of the longer lifetime components (I_3 less than 1% and I_4 less than 3%) are much smaller than the other two components. The longer lifetime components, of τ_3 about 2 ns for either sample and of τ_4 equal to 20 and 28 ns for the HDZ and EDS samples, respectively, are associated with the annihilation of positrons in ortho-positronium (o-Ps) states. The formation of positronium requires the existence of free volumes in the structure of the samples. According to the semiempirical correlation between the ortho-positronium lifetime and the radius of the open volume expressed in [49] we can predict, based on the τ_4 component, the presence of pore space in these samples with an average radius of approximately 1.5 nm. In fact, residual porosity with dimension of a few nanometers is often observed in compacted nanopowder materials [8, 50] and the existence of positronium is intimately related to the cavities between crystallites. From the components of lifetime τ_3 equal to 1.9 and 2.0 ns (for the HDZ and EDS samples, respectively), and according to the Tao–Eldrup model [51] we can identify a second group of voids with radius of approximately 0.6 nm. However, due to the small values of the intensity I_3 (see table 1) there is also the possibility that this component is an artifact of the broad size distribution of cavities.

Also, from table 1 it can be seen that most of the positrons implanted in the zirconia samples annihilate from two different states associated with lifetime components τ_1 and τ_2, which are related to different positron annihilation centers. Furthermore, the lifetimes of these components are distinctly different for the two samples. In either case, the corresponding τ_1 and τ_2 values are also significantly longer to the theoretically determined lifetime, τ_{bulk}, for a delocalized positron at the perfect lattice (equal to 152 ps or 179 ps by the PSN and CG methods, respectively). Hence, the observed τ_1 and τ_2 lifetimes are consistent with trapping and annihilation of positrons at open-volume defects in a saturation trapping regime. More specifically, the τ_1 lifetime component of 187 ps (HDZ sample) and 225 ps (EDS sample) is probably associated with Zr-monovacancy defects, the exact nature of which remains to be identified. These τ_1 values are comparable to calculated lifetimes of cation-monovacancy defects in several other oxides [17, 52], including the stabilized cubic phase of zirconia [8, 19]. Furthermore, the present τ_1 lifetimes are close to previous PAS measurements in various zirconia phases: in single-crystal samples of yttria-stabilized zirconia a single lifetime component of 175 ps was resolved [8]. It was argued that it originated from Zr vacancies. In the same study lifetime values of about 185 ps were reported for pressure-compacted zirconia nanopowders. Similarly, for stabilized-zirconia sintered ceramic samples. They were attributed to vacancy-type defects located at the space-charge layers along the grain boundaries in these nanocrystalline specimens. For those specimens with large grain sizes the measured lifetimes contained appreciable contributions from positrons trapped at vacancies inside the grains [8]. The concentration of vacancy-type defects in all these zirconia samples was relatively very high. In fact, a positron diffusion length of ≈ 9 nm was observed in single crystals of yttria-stabilized zirconia [8]. A similar positron diffusion length was observed for a single crystal of cubic zirconia [53]. These very small values for the positron diffusion length give evidence that positrons annihilate from a trapped state at defects and consequently the defect concentration must be high. For the sintered ceramics samples the observed lifetime component of 185 ps was attributed to annihilation at vacancy-type defects situated in the grain boundaries and also inside the grains. The lifetime components associated with the annihilation at vacancies inside the grains and in the grain boundaries should be different but closely spaced. This makes it practically impossible to distinguish them. The component coming from annihilation related to grain boundaries is expected to have a higher value [8].

Also, in another study on single-crystal and stabilized-zirconia sintered ceramic samples [54], a single lifetime component of approximately 184 ps was reported for the crystal samples. It was attributed to annihilation of positrons inside the grains and related to structural defects. A similar lifetime component was observed in ceramic samples and was attributed to defects inside the grains and to defects related to grain boundaries.

The lifetime component τ_1 (225 ps) (see table 1) for the EDS powder sample (of 17 nm grain size) is higher, to that of the HDZ powder sample (of 57 nm grain size), which is 187 ps. The intensity I_1 of this lifetime component for both samples is relatively similar (74.6% for the HDZ sample and 70.6% for the EDS sample). This result suggests that, owing to the small grain size of the EDS sample comparatively to the HDZ sample, the contribution of annihilation at vacancy defects at the grain boundaries is probably more significant in the case of EDS sample. The HDZ sample is characterized by a larger grain size, thus more annihilation at vacancy defects inside the grains must occur, leading to a smaller positron lifetime.

The second component with lifetime τ_2 (equal to 433 and 468 ps) is consistent with the trapping and annihilation of positrons in open-volume defects consisting of clusters of few monovacancies. In fact, it is well known that in nanocrystalline materials, due to the small grain size, the grain boundaries represent an important volume fraction of the material and possess a disordered structure with a high concentration of open-volume defects [8, 55, 56]. Due to the small grain size of the nanocrystallites in these samples, the implanted positrons can, after thermalization, reach by thermal diffusion the grain boundaries and be trapped at this kind of defects at the grain intersections [8, 55, 56].

3.3. Zirconium monovacancy: formation energies and positron lifetimes

The Zr ions in monoclinic zirconia have a seven-fold oxygen coordination [28]. In contrast, the O ions have a mixed three- and four-fold cation coordination. The Zr–O distances were found to range from 2.05 to 2.29 Å using the present LDA

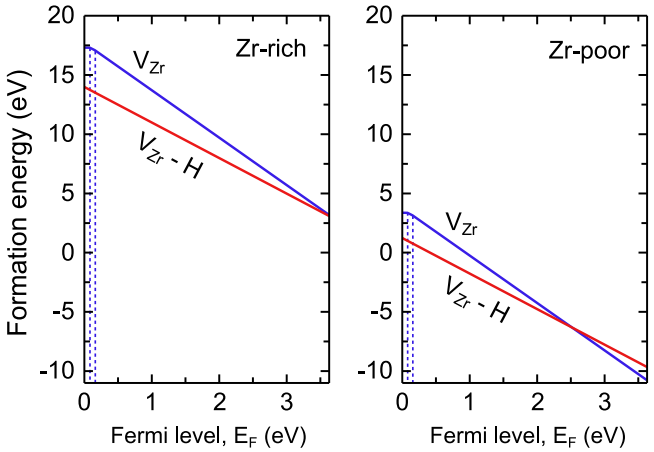

Figure 1. Formation energy of the Zr monovacancy (blue color) and of the vacancy–hydrogen complex (red color) as a function of the Fermi level in the theoretical gap, for Zr-rich and Zr-poor conditions. The vertical lines are the thermodynamic charge-transition levels (see text). The results were obtained using the LDA functional. The energy reference for the Fermi-level positions is the valence-band maximum, E_V.

DFT functional and assuming the experimental lattice parameters for the monoclinic lattice. Within the nearest-neighbor shell of a Zr ion the two nearest O ions have a three-fold cation coordination.

The Zr monovacancy was created by removing a single Zr atom from the supercell. Energy optimization at constant volume led to the minimum-energy ground-state configurations of the vacancy for each charge state. The resulting formation energy as a function of the Fermi level in the theoretical (LDA) gap was determined according to equation (1) and is plotted in figure 1 for both Zr-rich and Zr-poor conditions. Similarly to a previous first-principles study [6] the –4 state is the thermodynamically stable charge state in most of the band gap. The $\epsilon(-3/-4)$ charge-transition level lies very close to the valence band; at 0.15 eV above E_V. The neutral charge state is only stable within a very narrow region near E_V, with the $\epsilon(0/-3)$ level lying at 0.08 eV above E_V. The V_{Zr}^{-4} configuration is shown in detail in figure 2(a). The local environment of the vacancy is characterized by strong outward displacements of the oxygen nearest neighbors, in the range from 0.11 to 0.29 Å, away from the vacancy center. The two closest oxygen neighbors possess a three-fold cation coordination and are denoted by the symbols X and Y in figure 2(a). The distances of O_X and O_Y to the vacancy center are equal to 2.16 and 2.25 Å, respectively.

Calculations based on TCDFT and the PSN scheme were then subsequently carried out for the Zr monovacancy in its most stable state, V_{Zr}^{-4}. The results are summarized in table 2. The plot of the real-space positron density (see figure 3(a)) shows that the negatively-charged bare Zr monovacancy is a strong trapping site for a positron. The latter is localized at the vacancy site with almost 60% of its density found within the nearest-neighbor shell. The corresponding positron-vacancy binding energy, E_{bind}^{+}, was also calculated. Formally, E_{bind}^{+} is obtained as the energy difference of the total (system and positron) interaction energies with the positron present in the perfect-lattice and defect supercells, respectively. E_{bind}^{+} was found equal to -1.64 eV, something that means that the positron is bound to the vacancy.

A positron lifetime of 226 ps was obtained for the V_{Zr}^{-4} defect, a value which is much longer than τ_{bulk}, but matches very well the PAS lifetime measurements of the EDS powder (see table 1). All these findings clearly point out that one of the defects which causes positron trapping in monoclinic zirconia is the fully ionized Zr monovacancy. The calculated lifetime is similar in magnitude to lifetimes of Zr monovacancies in the stabilized cubic phase of zirconia determined with the same PSN method [19]. Furthermore, it is longer compared to the reported lifetime of the Zr monovacancy in monoclinic zirconia obtained by means of TCDFT and of a similar LDA electron–positron correlation scheme [7]. More specifically, the corresponding lifetime was equal to 202 ps. This difference with the earlier calculations could originate from the fact that the previous study assumed a rigid-lattice approximation where structural relaxation effects were ignored [7]. Furthermore, the charged state of the vacancy was assumed to be neutral [7]. Both of these approximations lead to smaller free volume around the vacancy defect and this may explain the comparatively shorter lifetime reported in that work [7].

The lifetime for the Zr monovacancy was also determined using gradient corrections. It was found equal to 304 ps, a value which exceeds considerably the PSN result. A shorter lifetime of 251 ps was obtained by the GC scheme by taking the random-phase approximation (RPA) limit [15, 44] in the enhancement factor, $g(n_+, n_-)$. Both of these GC-based lifetime values are consistently larger to the experimental τ_1 lifetimes obtained for the HDZ and EDS powders (see table 1).

3.4. Vacancy–hydrogen defect complexes: formation energies and positron lifetimes

Previous first-principles calculations demonstrated that isolated interstitial hydrogen is an amphoteric defect in monoclinic zirconia with its pinning level, $\epsilon(+/-)$, lying deep inside the band gap [58]. It was also shown that hydrogen binds more favorably to the three-fold coordinated oxygen ions, forming with them hydroxide-ion (O–H) configurations [59]. Corresponding O–H configurations with hydrogen binding to four-fold coordinated oxygen ions were also found to be possible, however, they were of higher energy [59].

In the present study defect association of the Zr monovacancy with interstitial hydrogen was explored by considering various trials sites for the hydrogen near the vacancy. In principle, all seven neighboring oxygen ions can be potential bonding partners. Indeed, hydrogen was found to bind to each one of these seven oxygen neighbors. The final configurations, however, were not isoenergetic. The energy minimization showed that hydrogen binds more favorably to the three-fold coordinated oxygen ion which resides closer to the Zr-vacancy site (the ion marked with the symbol X in figure 2). The formation energy of the vacancy–hydrogen defect complex was determined by taking into account of all

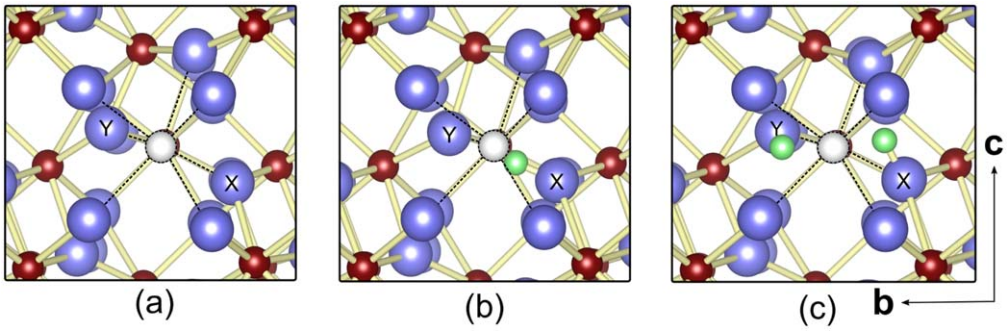

Figure 2. Atomistic structures of different vacancy defects: (a) Zr monovacancy, V_{Zr}^{-4}. (b) $(V_{Zr} - H)^{-3}$ defect complex. (c) $(V_{Zr} - 2H)^{-2}$ defect complex. The chemical elements are represented as: larger blue spheres for oxygen, smaller red spheres for zirconium and the small green spheres for hydrogen. The small white dashed circle denotes the Zr-vacancy site and is connected to its oxygen nearest neighbors by thin dashed lines. The view is along the lattice vestor **a**.

Table 2. Positron binding energies E_{bind}^{+} (in eV) and lifetimes τ (in ps) of bare and hydrogenated Zr monovacancies. The τ_{PSN} values in parentheses are lifetime results taking into account the positron-induced forces as well. The second set of τ_{GC} values were obtained using the RPA limit in the enhancement factor. The energies E_{bind}^{+} were determined using the PSN scheme.

Defect	E_{bind}^{+}	τ_{PSN}	τ_{GC}
V_{Zr}^{-4}	−1.64	226 (226)	304/251
$(V_{Zr} - H)^{-3}$	−1.10	207 (213)	277/235
$(V_{Zr} - 2H)^{-2}$	−0.53	186 (196)	253/220

possible charge states of the vacancy and the hydrogen defects, thus fully allowing mutual charge compensation. The final results are displayed in figure 1. It can be seen that the thermodynamically stable charge state of the $(V_{Zr} - H)$ defect complex is the $q = -3$ for all Fermi-level positions in the gap. Figure 2(b) depicts the detailed atomistic structure of the lowest-energy $(V_{Zr} - H)^{-3}$ configuration. The corresponding O–H bond length was found equal to 0.99 Å with the hydrogen residing at a distance of 1.36 Å away from the vacancy center.

Additional calculations were also performed to quantify the binding of the hydrogen to the vacancy, namely the stability of the defect complex against dissociation into its constituent defects, the bare monovacancy V_{Zr}^{-4} and the positively-charged interstitial hydrogen, H^{+}. The binding energy, E_b, is obtained as the balance of the respective formation energies, according to:

$$E_b = \Delta E_{form}[(V_{Zr} - H)^{-3}] - \Delta E_{form}[V_{Zr}^{-4}] - \Delta E_{form}[H^{+}]. \quad (4)$$

Thus, a negative sign for E_b means that the defect complex is stable against dissociation. The calculated binding energy for the lowest-energy $(V_{Zr} - H)^{-3}$ configuration was found equal to −1.24 eV; therefore the defect complex is stable with respect to an isolated interstitial H^{+} and a bare Zr vacancy, V_{Zr}^{-4}.

The positron lifetime for the $(V_{Zr} - H)^{-3}$ defect was found equal to 207 ps using the PSN scheme. Thus, hydrogen has a noticeable effect by decreasing by almost 8% the lifetime of the Zr monovacancy. Consideration of the positron-induced forces has a small effect by increasing slightly the lifetime by 6 ps (see table 2). The GC-based lifetimes were found to be much longer with respect to the PSN results.

The corresponding positron binding energy was again found to be negative, and equal to −1.10 eV, suggesting that the Zr vacancy (despite being bound to a hydrogen atom) can still act as a positron trapping center. Visualization of the positron density near the defect verifies this. The resulting positron density for the $(V_{Zr} - H)^{-3}$ vacancy complex is shown in figure 3(b). The positron remains localized near the vacancy, although with its center of gravity displaced away from the vacancy center owing to the mutual repulsion with the neighboring hydrogen.

Adding a second hydrogen atom in the vicinity of the Zr vacancy was further considered. Examination of all possible sites for the second hydrogen showed that it eventually binds more favorably to the oxygen ion denoted by *Y* in figure 2(c). This is the second nearest oxygen neighbor to the vacancy and similarly to O_X it also possesses a three-fold cation coordination. The incorporation of the second hydrogen atom to the existing $(V_{Zr} - H)^{-3}$ complex, however, entails strong structural relaxations whereby the first hydrogen atom displaces as much as 0.89 Å from its initial equilibrium position (see figure 2). In the final relaxed configuration the two hydrogen atoms reside at 1.43 and 1.35 Å away from the vacancy center. The hydrogen–hydrogen distance in this configuration is equal to 2.25 Å. The binding energy for the second hydrogen atom was again found to be negative and equal to −0.99 eV. Thus, there is still a driving force for hydrogen atoms to be attached to existing vacancy–hydrogen complexes and form new stable defect complexes, $(V_{Zr} - 2H)^{-2}$, with a double hydrogen occupancy.

These complexes are also negatively charged and thus capable of trapping positrons. The positron binding energy to the $(V_{Zr} - 2H)^{-2}$ defect is negative, albeit much smaller now (equal to −0.53 eV) (see table 2), again suggesting that these defects can still be trapping centers for positrons, although not as deep. The resulting real-space positron density plotted in figure 3(c) clearly confirms this. It can be seen that the positron is localized at the Zr-vacancy site, although it has lost much of its intensity. The corresponding density is

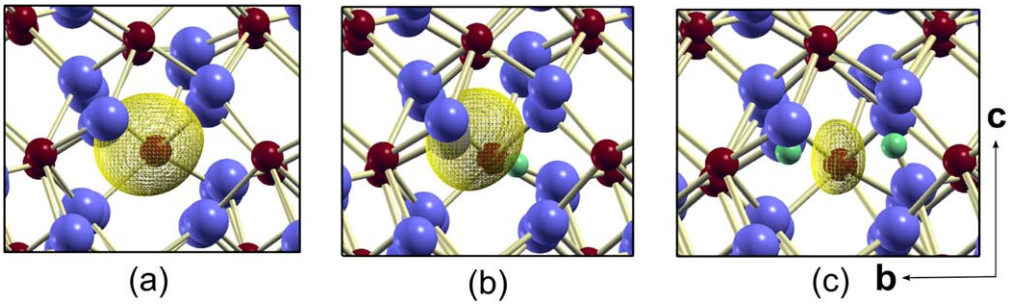

Figure 3. Real-space positron densities (in yellow) of the vacancy defects, obtained within the PSN scheme. (a) Zr monovacancy, V_{Zr}^{-4}. (b) $(V_{Zr} - H)^{-3}$ defect complex. (c) $(V_{Zr} - 2H)^{-2}$ defect complex. The densities are shown for an isosurface value of 0.0045 (a.u.)$^{-3}$ which corresponds to 58%, 66% and 88% of the maximum positron density for the defects shown in (a), (b) and (c), respectively. The view is along the lattice vector **a**. The figure was generated with the help of the XCRYSDEN program [57].

affected by the two hydrogen atoms nearby and adopts an asymmetrical shape of an ellipsoid with its longer axis pointing away from either hydrogen.

The calculated positron lifetime for the lowest-energy $(V_{Zr} - 2H)^{-2}$ configuration was found equal to 186 ps. Again, the effect of positronic forces was moderate; they led to a small increase of the lifetime by 10 ps. These lifetime values are close to the measured lifetime component, τ_1, from the HDZ powder (see table 1). This finding indicates the presence of hydrogen in these samples; the Zr vacancy decorated by hydrogen is very likely the defect which causes positron trapping in this case.

4. Conclusions

Positron trapping at Zr monovacancies in monoclinic zirconia was studied by means of two-component density-functional theory and experimental measurements of positron-annihilation spectra. The obtained positron lifetime for the fully ionized Zr monovacancy using an LDA-based electron–positron correlation approach was found equal to 226 ps, almost 50% longer to the perfect-lattice value. Additional calculations were also performed to appraise the role of hydrogen which is by far the most ubiquitous impurity in oxides. It was shown that hydrogen atoms bind favourably to three-fold coordinated oxygen ions inside the nearest-neighbor shell of the Zr monovacancy. Decoration of the Zr vacancy by one and two hydrogen atoms affected the ability of the vacancy to trap positrons by decreasing the defect-positron binding energies and leading to shorter positron lifetimes by as much as 40 ps. The theoretical lifetime results were verified by PAS measurements for two different sets of powder samples which revealed positron annihilation from distinct defect states with lifetime components of 187 and 225 ps.

Acknowledgments

The authors acknowledge financial support from FEDER (Programa Operacional Factores de Competitividade COMPETE) and from FCT Portugal—Fundação para a Ciência e Tecnologia under the UID/FIS/04564/2016 and PTDC/FIS/102722/2008 projects. The computer resources of the Department of Physics of the University of Coimbra were used, including the Navigator cluster at the Laboratory for Advanced Computing.

ORCID iDs

A G Marinopoulos https://orcid.org/0000-0002-1951-4832

References

[1] Heuer A and Hobbs L W (ed) 1981 *Science and Technology of Zirconia* (*Advances in Ceramics* vol 3) (Westerville, OH: The American Ceramic Society)
[2] Robertson J 2006 *Rep. Prog. Phys.* **69** 327–96
[3] Afanasev V V and Stesmans A 2004 *J. Appl. Phys.* **95** 2518–26
[4] Foster A S, Sulimov V B, Lopez Gejo F, Shluger A L and Nieminen R M 2001 *Phys. Rev.* B **64** 224108
[5] Robertson J, Xiong K and Falabretti B 2005 *IEEE Trans. Device Mater. Reliab.* **5** 84–9
[6] Zheng J X, Ceder G, Maxisch T, Chim W K and Choi W K 2007 *Phys. Rev.* B **75** 104112
[7] Melikhova O, Kuriplach J, Čížek J, Procházka I, Anwand W, Brauer G, Konstantinova T E and Danilenko I A 2007 *Phys. Status Solidi* c **4** 3831–4
[8] Čížek J, Melikhova O, Procházka I, Kuriplach J, Kužel R, Brauer G, Anwand W, Konstantinova T E and Danilenko I A 2010 *Phys. Rev.* B **81** 024116
[9] Ou X, Kögler R, Zhou H-B, Anwand W, Grenzer J, Hübner R, Voelskow M, Butterling M, Zhou S and Skorupa W 2012 *Phys. Rev.* B **86** 224103
[10] Puska M J and Nieminen R M 1994 *Rev. Mod. Phys.* **66** 841–97
[11] Dupasquier A and Mills A P Jr. (ed) 1995 *Positron Spectroscopy of Solids* (Amsterdam, Oxford, Tokyo, Washington DC: IOS Press)
[12] Tuomisto F and Makkonen I 2013 *Rev. Mod. Phys.* **85** 1583–631
[13] Chakraborty B 1981 *Phys. Rev.* B **24** 7423–6
[14] Chakraborty B and Siegel R W 1983 *Phys. Rev.* B **27** 4535–52
[15] Borónski E and Nieminen R M 1986 *Phys. Rev.* B **34** 3820–31
[16] Hansen H E, Nieminen R M and Puska M J 1984 *J. Phys. F: Met. Phys.* **14** 1299–316
[17] Brauer G *et al* 2009 *Phys. Rev.* B **79** 115212

[18] Melikhova O, Kuriplach J, Čížek J, Prochazka I, Brauer G and Anwand W 2010 *J. Phys.: Conf. Ser.* **225** 012035
[19] Marinopoulos A G 2019 *J. Phys.: Condens. Matter* **31** 315503
[20] Kilic C and Zunger A 2002 *Appl. Phys. Lett.* **81** 73
[21] Van de Walle C G and Neugebauer J 2003 *Nature* **423** 626–8
[22] Xiong K, Robertson J, Robertson J and Clark S J 2007 *J. Appl. Phys.* **102** 083710
[23] Li H and Robertson J 2014 *J. Appl. Phys.* **115** 203708
[24] Janotti A and Van de Walle C G 2007 *Nat. Mater.* **6** 44–7
[25] Youssef M and Yildiz B 2012 *Phys. Rev.* B **86** 144109
[26] Youssef M and Yildiz B 2014 *Phys. Chem. Chem. Phys.* **16** 1354
[27] Varley J B, Peelaers H, Janotti A and Van de Walle C G 2011 *J. Phys.: Condens. Matter* **23** 334212
[28] Hann R E, Suitch P R and Pentecost J L 1985 *J. Am. Ceram. Soc.* **68** 285
[29] Hohenberg P and Kohn W 1964 *Phys. Rev.* **136** B864–71
[30] Kohn W and Sham L J 1965 *Phys. Rev.* **140** A1133–8
[31] Blöchl P E 1994 *Phys. Rev.* B **50** 17953–79
[32] Perdew J P and Wang Y 1992 *Phys. Rev.* B **45** 13244–9
[33] Perdew J P, Burke K and Ernzerhof M 1996 *Phys. Rev. Lett.* **77** 3865–8
[34] Kresse G and Hafner J 1993 *Phys. Rev.* B **47** 558–61
[35] Kresse G and Hafner J 1994 *Phys. Rev.* B **49** 14251–69
[36] Kresse G and Furthmüller J 1996 *Phys. Rev.* B **54** 11169–86
[37] Kresse G and Joubert D 1999 *Phys. Rev.* B **59** 1758–75
[38] Monkhorst H and Pack J 1976 *Phys. Rev.* B **13** 5188–92
[39] Matsunaga K, Tanaka T, Yamamoto T and Ikuhara Y 2003 *Phys. Rev.* B **68** 085110
[40] Gonze X *et al* 2016 *Comput. Phys. Commun.* **205** 106
[41] Puska M J, Seitsonen A P and Nieminen R M 1995 *Phys. Rev.* B **52** 10947–61
[42] Wiktor J, G Jomard and Torrent M 2015 *Phys. Rev.* B **92** 125113
[43] Holzwarth N A W, Tackett A R and Matthews G E 2001 *Comput. Phys. Commun.* **135** 329
[44] Barbiellini B, Puska M J, Torsti T and Nieminen R M 1995 *Phys. Rev.* B **51** 7341–4
[45] Barbiellini B, Puska M J, Korhonen T, Harju A, Torsti T and Nieminen R M 1996 *Phys. Rev.* B **53** 16201–13
[46] Kansy J 1996 *Nucl. Instruments Methods Phys. Res.* A **374** 235–44
[47] Surbeck H 1977 *Helv. Phys. Acta* **50** 705–21
[48] Kuriplach J and Barbiellini B 2014 *Phys. Rev.* B **89** 155111
[49] Ito K, Nakanishi H and Ujihira Y 1999 *J. Phys. Chem.* B **103** 4555
[50] Ito K, Yagi Y, Hirano S, Miyayama M, Kudo T, Kishimoto A and Ujihira Y 1999 *J. Ceram Soc. Japan* **107** 123–7
[51] Eldrup M, Lightbody D and Sherwood J N 1981 *J. Chem. Phys.* **63** 51–8
[52] Keeble D J, Wicklein S, Dittmann R, Ravelli L, Mackie R A and Egger W 2010 *Phys. Rev. Lett.* **105** 226102
[53] Grynszpan R I, Saude S, Mazerolles L, Brauer G and Anwand W 2007 *Radiat. Phys. Chem.* **76** 333–6
[54] Gonzalo-Juan I, Parente P, Sanchez-Herencia A J, Rubio F, Pareja R and Ferrari B 2011 *Solid State Ion.* **190** 67–74
[55] Staab T E M, Krause-Rehberg R and Kieback B 1999 *J. Mater. Sci.* **34** 3833–51
[56] Birringer R 1989 *Mater. Sci. Eng.* A **117** 33–43
[57] Kokalj A 2003 *Comput. Mater. Sci.* **28** 155–68
[58] Lyons J L, Janotti A and Van de Walle C G 2011 *Microelectron. Eng.* **88** 1452–6
[59] Mantz Y A and Gemmen R S 2010 *J. Phys. Chem.* C **114** 8014